Entanglement between two spatially separated atomic modes

Karsten Lange,[1] Jan Peise,[1] Bernd Lücke,[1] Ilka Kruse,[1] Giuseppe Vitagliano,[2,3] Iagoba Apellaniz,[3] Matthias Kleinmann,[3,4] Géza Tóth,[3,5,6] Carsten Klempt[1]*

Modern quantum technologies in the fields of quantum computing, quantum simulation, and quantum metrology require the creation and control of large ensembles of entangled particles. In ultracold ensembles of neutral atoms, nonclassical states have been generated with mutual entanglement among thousands of particles. The entanglement generation relies on the fundamental particle-exchange symmetry in ensembles of identical particles, which lacks the standard notion of entanglement between clearly definable subsystems. Here, we present the generation of entanglement between two spatially separated clouds by splitting an ensemble of ultracold identical particles prepared in a twin Fock state. Because the clouds can be addressed individually, our experiments open a path to exploit the available entangled states of indistinguishable particles for quantum information applications.

The progress toward large ensembles of entangled particles is pursued along two different paths. In a bottom-up approach, the precise control and characterization of small systems of ions, atoms in optical lattices, and photons is pushed toward increasingly large system sizes, reaching entangled states of 14 ions (1), 4 atomic lattice sites (2), or 10 photons (3). Complementary, large numbers of up to 3000 mutually entangled ultracold atoms (4–6) can be generated, for which the state characterization is advanced top-down toward resolving correlations on the single-particle level. Because the atoms cannot be addressed individually, ultracold atomic ensembles are controlled by global ensemble parameters, such as the total spin. Ideally, the atoms are indistinguishable, either with respect to the observable, such as the spin in hot vapor cells (7), or in all quantum numbers in Bose-Einstein condensates (BECs) (8–13). Is it possible to make these particles distinguishable—and addressable—again, while keeping the high level of entanglement?

The generation of entanglement in these systems is deeply connected with the fundamental indistinguishability of the particles (14). For example, two indistinguishable bosons 1 and 2,

which are prepared in two independent modes a and b, are described by an entangled triplet state $\frac{1}{\sqrt{2}}(|a\rangle_1|b\rangle_2 + |b\rangle_1|a\rangle_2)$, owing to bosonic symmetrization. Although this type of entanglement seems to be artificial, the state presents a resource for violating a Bell inequality (15). Equivalently, an ensemble containing the same number of distinguishable spin-up and spin-down atoms is not necessarily entangled, whereas a twin Fock state, the corresponding ensemble with indistinguishable bosons, exhibits full many-particle entanglement (16, 17). This form of entanglement is directly applicable for atom interferometry beyond the standard quantum limit (11). However, most quantum information tasks require an individual addressing of subsystems. Despite the experimental progress in entanglement creation in BECs—including the demonstration of Einstein-Podolsky-Rosen (EPR) correlations (18) and Bell correlations (19–21), as well as the demonstration of strongly correlated momentum states (22–24)—a proof of entanglement between spatially separated and individually addressable subsystems has not been realized so far. The possible applications of such a resource range from spatially resolved quantum metrology to tests for fundamental

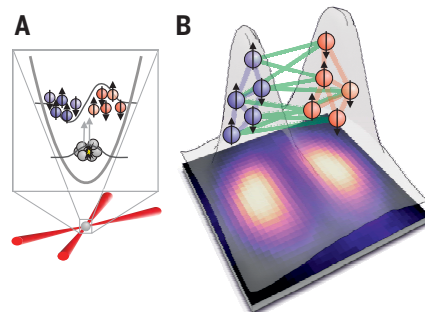sources of decoherence or Bell tests of quantum nonlocality.

Here, we report the creation of particle entanglement in an ensemble of up to 5000 indistinguishable atoms and prove entanglement between two spatially separated clouds.

Our experiments started with the preparation of a ^{87}Rb BEC in a crossed-beam optical dipole trap. The ensemble of 20,000 particles was transferred to the hyperfine level $F = 1$, $m_F = 0$. Spin-changing collisions created up to 5000 entangled atoms in the Zeeman levels $m_F = \pm 1$, which resided in a spatially excited mode of the dipole trap (25, 26) (Fig. 1). The output state consisted of a superposition of twin Fock states with varying total number of atoms $N = N_{+1} + N_{-1}$. Each twin Fock state is characterized by an equal number of atoms $N_{+1} = N_{-1}$ in the two Zeeman levels $m_F = \pm 1$ (11). Because the total number of particles N was measured during detection, the system was well described by a single twin Fock state with a definite particle number. Self-similar expansion (26) allowed for an imaging of the undistorted but magnified density profiles. An inhomogeneous magnetic field separated the atoms in order to record the atomic densities for each Zeeman level.

The spatially excited mode of the ensembles in $m_F = \pm 1$ provides a natural splitting into a left and right cloud along a line of zero density. Hence, we divided the initial twin Fock state into two spatially separated parts, $|a\rangle$ (left side) and $|b\rangle$ (right side). This process can be described as a beam splitter of the initially populated antisymmetric input mode $\frac{1}{\sqrt{2}}(|a\rangle - |b\rangle)$. The splitting introduces additional quantum noise caused by a coupling with the (empty) symmetric input mode $\frac{1}{\sqrt{2}}(|a\rangle + |b\rangle)$. In principle, an ideal twin Fock state shows a maximal entanglement depth (16); all atoms that make up a twin Fock state are entangled with one another. Therefore, any splitting results in the appearance of quantum correlations between the clouds. Such a creation of entanglement is analogous to so-called vacuum-class entanglement (27) in optics, in which a single-mode squeezed laser beam is coupled to a vacuum state on a beam splitter, creating entanglement between the two output modes (28).

The resulting quantum correlations can be visualized on the multiparticle Bloch sphere (Fig. 2A). Here, the atoms in the levels $m_F = \pm 1$ are represented by spin-½ particles, whose spins $\mathbf{j}^{(k)}$ sum up to a total spin $\mathbf{J}$. On the Bloch sphere, the lines of latitude represent the number imbalance

Fig. 1. Generation of entanglement between two spatially separated atomic clouds. (**A**) A BEC of atoms in the Zeeman level $m_F = 0$ is prepared in a crossed-beam optical trap. Collisions generate entangled pairs of atoms in the levels $m_F = \pm 1$ (spin up/down) in the first spatially excited mode. The created multiparticle-entangled ensemble is naturally divided into two clouds (red and blue). (**B**) The atomic density profile obtained from an average over 3329 measurements is shown in the background. The entanglement between the two clouds (indicated schematically with green lines) can be detected by analyzing spin correlations.

between the two levels, and the lines of longitude represent the phase difference. An ensemble in a twin Fock state can be depicted as a ring on the Bloch sphere, characterized by a vanishing imbalance, $J_z = (N_{+1} - N_{-1})/2 = 0$, and an undetermined phase difference.

If we divide the cloud, the collective spins $\mathbf{J}^{(a)}$, $\mathbf{J}^{(b)}$ of the two parts have to sum up to the original collective spin of the full ensemble $\mathbf{J} = \mathbf{J}^{(a)} + \mathbf{J}^{(b)}$. Therefore, the z components of the collective spins are perfectly anticorrelated $J_z^{(a)} + J_z^{(b)} = 0$. Furthermore, because the spin length $|\mathbf{J}|$ is maximal, the collective spins of the two parts have to point in a similar direction in the x-y plane and thus have similar azimuthal angles $\phi^{(a)} \approx \phi^{(b)}$.

Hence, if the particle number difference of cloud b is measured to yield $J_z^{(b)}$, the conditioned state of cloud a satisfies $J_z^{(a)} = -J_z^{(b)}$. If the value $J_x^{(b)}$ is measured on cloud b, the state of cloud a has to fulfill $J_x^{(a)} \approx J_x^{(b)}$; if the value $J_y^{(b)}$ is measured on cloud b, the state of cloud a has to fulfill $J_y^{(a)} \approx J_y^{(b)}$. The different possible measurements on cloud b yield precise predictions for the measurement results of cloud a, which cannot be explained by a single quantum state that is independent of the chosen type of measurement. In this sense, the described system is analogous to the thought experiment by Einstein, Podolsky, and Rosen (29), in which entanglement is witnessed by the variances of the predictions (30, 31). Therefore, it should be possible to detect entanglement between the spatially separated parts of a twin Fock state.

To this end, we derived an entanglement criterion that optimally exploits the described spin correlations (32). The spin correlations are represented by prediction operators $\tilde{J}_z^+ = \tilde{J}_z^{(a)} + \tilde{J}_z^{(b)}$ and $\tilde{J}_m^- = \tilde{J}_m^{(a)} - \tilde{J}_m^{(b)}$ for $m = x, y$. Here, the x and y components are normalized so that the optimal value is 1, according to $\tilde{J}_m^{(n)} = \frac{J_m^{(n)}/j_n}{\mathcal{J}^{(n)}}$, with $\mathcal{J}^{(n)} = \left\langle \frac{(J_x^{(n)})^2 + (J_y^{(n)})^2}{j_n^2} \right\rangle^{\frac{1}{2}}$ and the spin length $j_n = N_n/2$ for $n = $ a, b. We arrive at a simple separability criterion

$$\left[(\Delta \tilde{J}_z^+)^2 + \frac{1}{2} \right] \times \left[\left\langle (\tilde{J}_x^-)^2 + (\tilde{J}_y^-)^2 \right\rangle \right] \geq f\left(\mathcal{J}^{(a)}, \mathcal{J}^{(b)} \right) \quad (1)$$

where $f(r, s) = \frac{(r^2 + s^2 - 1)^2}{rs}$. Any separable state, including mixtures of product states of the form $\sum_k p_k |\Psi_k^{(a)}\rangle\langle\Psi_k^{(a)}| \otimes |\Psi_k^{(b)}\rangle\langle\Psi_k^{(b)}|$ with a fluctuating number of particles, fulfills this inequality. A violation of this criterion indicates that the state is inseparable and therefore entangled. For perfectly symmetric states, as we would expect in the ideal case, the right-hand side (RHS) of Eq. 1 is equal to 1. Any deterioration from perfect symmetry is quantified by $\mathcal{J}^{(a)}$ and $\mathcal{J}^{(b)}$. Containing the characteristic product of the prediction uncertainties, our inequality for three-dimensional spins has similarities to the famous two-dimensional continuous-variable entanglement criteria (31, 33, 34), specifically to the EPR criterion (33). It presents a general entanglement criterion, which is particularly sensitive for a spatially separated twin Fock state.

An application of criterion in Eq. 1 requires an evaluation of the spin correlations between the two clouds a and b. The measurement results for $J_z^{(a)}$ and $J_z^{(b)}$ are readily obtained from the absorption images. The measurement of the orthogonal direction is performed with a sequence of resonant microwave pulses before the particle number detection (32). The pulses lead to an effective rotation of the spins by $\pi/2$. Because the microwave phase is independent of the atomic phases, the rotation yields a measurement of the spin component $J_\perp$ along an arbitrary angle in the x-y plane. Because our quantum state is symmetric under rotations around the z axis, both owing to the initial symmetry and the influence of magnetic field noise, the measured distributions of $J_\perp$ can be identified with both J_x and J_y.

The histograms of J_z and $J_\perp/j$ are shown in Fig. 2, B and C, for a mean total number of 3460 particles in both clouds together. The J_z data show the expected anticorrelation, whereas the $J_\perp$ measurements are strongly correlated. The strength of these correlations can be quantified by evaluating the prediction uncertainties—the width of the distributions in the diagonal directions in the histograms: $(\Delta \tilde{J}_z^+)^2$ and $\langle (\tilde{J}_\perp^-)^2 \rangle$.

The prediction variance $(\Delta \tilde{J}_z^+)^2$ is presented in Fig. 3A as a function of the total number of atoms. The shown fluctuations, obtained by subtracting independent detection noise (32), remain

Fig. 2. Spin correlations between the clouds a and b. (**A**) A twin Fock state is represented by a narrow ring on the equator of the multiparticle Bloch sphere (top, orange). When the system is split into two parts, a (left, blue) and b (right, red), the states in the individual subsystems gain uncertainty. However, a measurement of $J_z^{(b)}$ or $\phi^{(b)}$ on cloud b allows for a prediction of the measurement outcome of cloud a, so that $J_z^{(a)} = -J_z^{(b)}$ or $\phi^{(a)} \approx \phi^{(b)}$. (**B**) Histogram of 506 measurements of $J_z^{(a)}$ and $J_z^{(b)}$ for a mean total number of 3460 atoms. The data show the anticipated anticorrelation between $J_z^{(a)}$ and $J_z^{(b)}$. (**C**) The strong correlations between the angles $\phi^{(a)}$ and $\phi^{(b)}$ are recorded by a measurement of their projection on an arbitrary axis $J_\perp$ in the x-y plane. The histogram of $J_\perp^{(a)}/j_a$ and $J_\perp^{(b)}/j_b$ is drawn from 487 measurements.
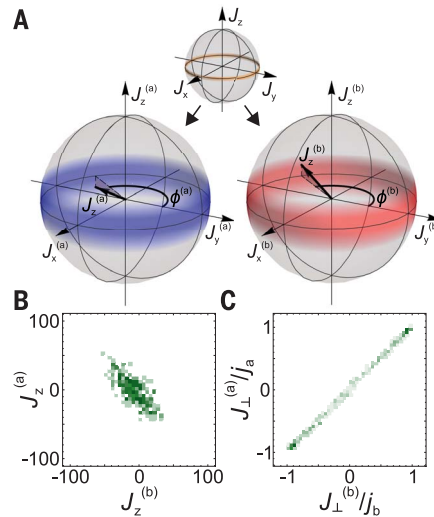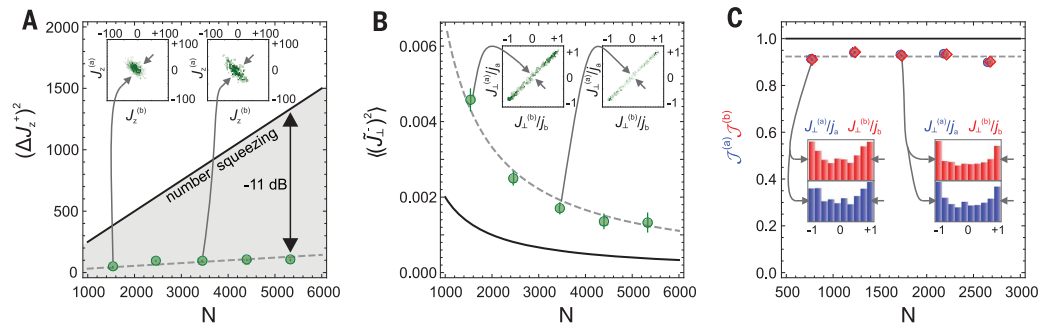
Fig. 3. Spin correlations as a function of the total number of atoms N. (**A**) The prediction variance $(\Delta \tilde{J}_z^+)^2$ (green circles) surpasses the shot-noise limit (black solid line), indicating number squeezing of up to $-11.0(5)$ dB. The number-dependent detection noise is modeled by a linear fit (gray dashed line). (**B**) The fluctuations $\langle (\tilde{J}_\perp^-)^2 \rangle = \langle (\tilde{J}_x^-)^2 \rangle = \langle (\tilde{J}_y^-)^2 \rangle$ (green circles), corresponding to the phase prediction variance in the experiment, show excess noise, which increases the standard deviation by a factor of 1.8 (gray dashed line) above the shot-noise limited case (black solid line). (**C**) $\mathcal{J}^{(a)}$ and $\mathcal{J}^{(b)}$ quantify the symmetry of the states. The value 1 for purely symmetric states is indicated with the black line, and the mean experimental value is indicated with the gray dashed line. In (A) to (C), we binned our experimental data into sets of 1000 atoms. N corresponds to the mean number of atoms in each set. The error bars represent 1 standard deviation of the statistical fluctuations and are obtained via a bootstrapping method (32).
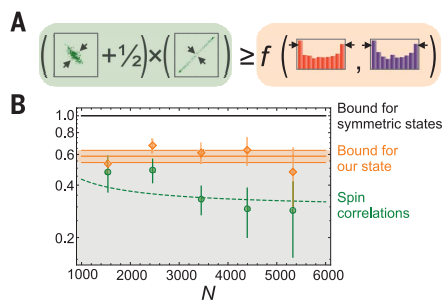
Fig. 4. Violation of the separability criterion as a function of the total number of atoms N. (**A**) Pictorial representation of the criterion in Eq. 1. (**B**) The black line represents the RHS of Eq. 1 for the ideal case. The orange line represents the mean of the experimental results (orange diamonds) of the RHS of Eq. 1, where the spin length is reduced. The green circles show the experimental results for the LHS of Eq. 1 . The dashed green line indicates the prediction of the LHS corresponding to the gray lines in Fig. 3. The spin correlations clearly violate the criterion by 2.8 standard deviations at a mean total number of 3460 atoms. The error bars and shaded orange area indicate 1 standard deviation and are obtained via a bootstrapping method (32).

well below the shot-noise limit and are equivalent to a number squeezing of –11.0(5) dB. The orthogonal quantities (Fig. 3B) are slightly influenced by small position fluctuations of the clouds, increasing the standard deviation by a factor of 1.8 above shot noise. The quantities $\mathcal{J}^{(a)}$ and $\mathcal{J}^{(b)}$ are shown in Fig. 3C. We obtained a value of up to 0.94, close to the ideal value of 1, indicating a sufficiently clean preparation of an almost symmetric state.

From these results, we could test a violation of the separability criterion. In Fig. 4B, the orange diamonds correspond to an evaluation of the RHS of the criterion (Eq. 1), which would ideally be 1 (black line). For most values of N, the left-hand side (LHS), represented in Fig. 4B by the green circles, is well below the RHS, signaling entanglement in the system. At the best value of the total number of 3460 atoms, the experimental data violate the separability criterion by 2.8 standard deviations. Therefore, our measurements cannot result from classical correlations and prove the generation of entanglement

between spatially separated clouds from particle-entangled, indistinguishable atoms.

The presented creation of spatial entanglement opens a path to create highly entangled quantum states in spatially separated modes for a broad range of applications. This includes the field of quantum metrology, where our results can be applied in order to obtain an improved spatial resolution—for example, in the sensing of electromagnetic fields. Owing to the possibility of addressing the separated modes—for example, with Raman beams or spatially modulated light shifts—the created states are a resource for quantum information protocols. For example, it presents a resource for the synthesis of any pure symmetric state with only single-particle projective measurements (35, 36). Moreover, the spatially separated twin Fock state carries nonlocal EPR and Bell correlations. The presented experimental scheme can be extended to a multiparticle Bell test of quantum mechanics with the addition of local addressing of the two modes and a single-particle–resolving atom counting (37). Last, if the created twin Fock state is fully separated into single atoms—for example, in an optical lattice—all constituent particles become individually addressable.

Complementary to our work, in (38), spatially distributed multipartite entanglement has been observed, whereas spatial entanglement patterns were observed in (39).

REFERENCES AND NOTES

1. T. Monz et al., Phys. Rev. Lett. **106**, 130506 (2011).
2. R. Islam et al., Nature **528**, 77–83 (2015).
3. X.-L. Wang et al., Phys. Rev. Lett. **117**, 210502 (2016).
4. R. McConnell, H. Zhang, J. Hu, S. Ćuk, V. Vuletić, Nature **519**, 439–442 (2015).
5. F. Haas, J. Volz, R. Gehr, J. Reichel, J. Estève, Science **344**, 180–183 (2014).
6. O. Hosten, N. J. Engelsen, R. Krishnakumar, M. A. Kasevich, Nature **529**, 505–508 (2016).
7. B. Julsgaard, A. Kozhekin, E. S. Polzik, Nature **413**, 400–403 (2001).
8. J. Estève, C. Gross, A. Weller, S. Giovanazzi, M. K. Oberthaler, Nature **455**, 1216–1219 (2008).
9. C. Gross, T. Zibold, E. Nicklas, J. Estève, M. K. Oberthaler, Nature **464**, 1165–1169 (2010).
10. M. F. Riedel et al., Nature **464**, 1170–1173 (2010).
11. B. Lücke et al., Science **334**, 773–776 (2011).
12. C. D. Hamley, C. S. Gerving, T. M. Hoang, E. M. Bookjans, M. S. Chapman, Nat. Phys. **8**, 305–308 (2012).
13. T. Berrada et al., Nat. Commun. **4**, 2077 (2013).
14. N. Killoran, M. Cramer, M. B. Plenio, Phys. Rev. Lett. **112**, 150501 (2014).
15. B. Yurke, D. Stoler, Phys. Rev. A **46**, 2229–2234 (1992).
16. B. Lücke et al., Phys. Rev. Lett. **112**, 155304 (2014).
17. X.-Y. Luo et al., Science **355**, 620–623 (2017).
18. J. Peise et al., Nat. Commun. **6**, 8984 (2015).
19. J. Tura et al., Science **344**, 1256–1258 (2014).
20. J. Tura et al., Ann. Phys. **362**, 370–423 (2015).
21. R. Schmied et al., Science **352**, 441–444 (2016).
22. R. Bücker et al., Nat. Phys. **7**, 608–611 (2011).
23. J. Lopes et al., Nature **520**, 66–68 (2015).
24. P. Dussarrat et al., Phys. Rev. Lett. **119**, 173202 (2017).
25. C. Klempt et al., Phys. Rev. Lett. **103**, 195302 (2009).
26. M. Scherer et al., Phys. Rev. Lett. **105**, 135302 (2010).
27. J. DiGuglielmo, B. Hage, A. Franzen, J. Fiurášek, R. Schnabel, Phys. Rev. A **76**, 012323 (2007).
28. T. Eberle et al., Phys. Rev. A **83**, 052329 (2011).
29. A. Einstein, B. Podolsky, N. Rosen, Phys. Rev. **47**, 777–780 (1935).
30. L.-M. Duan, G. Giedke, J. I. Cirac, P. Zoller, Phys. Rev. Lett. **84**, 2722–2725 (2000).
31. R. Simon, Phys. Rev. Lett. **84**, 2726–2729 (2000).
32. Materials and methods are available as supplementary materials.
33. M. D. Reid, Phys. Rev. A **40**, 913–923 (1989).
34. L.-M. Duan, A. Sørensen, J. I. Cirac, P. Zoller, Phys. Rev. Lett. **85**, 3991–3994 (2000).
35. W. Wieczorek et al., Phys. Rev. Lett. **103**, 020504 (2009).
36. N. Kiesel et al., Phys. Rev. A **81**, 032316 (2010).
37. F. Laloë, W. J. Mullin, Eur. Phys. J. B **70**, 377–396 (2009).
38. P. Kunkel et al., Science **360**, 413–416 (2018).
39. M. Fadel, T. Zibold, B. Décamps, P. Treutlein, Science **360**, 409–413 (2018).

Science

Entanglement between two spatially separated atomic modes

Karsten Lange, Jan Peise, Bernd Lücke, Ilka Kruse, Giuseppe Vitagliano, Iagoba Apellaniz, Matthias Kleinmann, Géza Tóth
and Carsten Klempt

Splitting the entanglement
When particles in a quantum mechanical system are entangled, a measurement performed on one part of the
system can affect the results of the same type of measurement performed on another part—even if these subsystems
are physically separated. Kunkel *et al.*, Fadel *et al.*, and Lange *et al.* achieved this so-called distributed entanglement in
a particularly challenging setting: an ensemble of many cold atoms (see the Perspective by Cavalcanti). In all three
studies, the entanglement was first created within an atomic cloud, which was then allowed to expand. Local
measurements on the different, spatially separated parts of the cloud confirmed that the entanglement survived the
expansion.
Science, this issue p. 413, p. 409, p. 416; see also p. 376

ARTICLE TOOLS	http://science.sciencemag.org/content/360/6387/416
SUPPLEMENTARY MATERIALS	http://science.sciencemag.org/content/suppl/2018/04/25/360.6387.416.DC1
RELATED CONTENT	http://science.sciencemag.org/content/sci/360/6387/376.full http://science.sciencemag.org/content/sci/360/6387/409.full http://science.sciencemag.org/content/sci/360/6387/413.full
REFERENCES	This article cites 40 articles, 7 of which you can access for free http://science.sciencemag.org/content/360/6387/416#BIBL
PERMISSIONS	http://www.sciencemag.org/help/reprints-and-permissions